Design and development of wobbling triboelectric nanogenerators for harvesting sustainable energy from wind and vibration

Ghaderiaram, Aliakbar; Schlangen, Erik; Fotouhi, Mohammad

DOI
10.1016/j.ecmx.2025.101037

Publication date
2025

Document Version
Final published version

Published in
Energy Conversion and Management: X

Energy Conversion and Management: X 26 (2025) 101037

Contents lists available at ScienceDirect

Energy Conversion and Management: X

journal homepage: www.sciencedirect.com/journal/energy-conversion-and-management-x

Design and development of wobbling triboelectric nanogenerators for harvesting sustainable energy from wind and vibration

Aliakbar Ghaderiaram *, Erik Schlangen, Mohammad Fotouhi

Materials and Environment, Delft University of Technology, Stevinweg 1, 2628 CN Delft, The Netherlands

ARTICLE INFO

Keywords:
TENG
Wobbling
Wind
Vibration
Energy harvester
Self-powered

ABSTRACT

This paper reports the development, optimization, and real-world application of an innovative wobbling triboelectric nanogenerator to harvest energy from wind or vibrations. The harvester features a spring-supported structure, purposely designed to become unbalanced and reversibly shift from a steady to a non-steady state in response to minimal wind or vibration stimuli. Unlike conventional wind turbines, this approach transforms wind energy into contact-separation events via a wobbling structure. The harvester's mechanisms are engineered to enhance power generation efficiency, optimizing parameters like electrode dimensions and contact-separation quality. Experimental findings showcase a maximum output power density of 1.6 W/m^2 under optimal conditions, employing a fixed suspending mechanism for heightened impact energy during contact. Moreover, the harvester efficiently charges a 3.7 V lithium-ion battery with over 4.5 μA, showcased in a self-powered light mast as a practical demonstration. The harvester provides cost-effectiveness by utilizing inexpensive, easily accessible materials without complex fabrication. This research paves the way for future exploration in integrating triboelectric nanogenerators with wobbling mechanisms, offering a promising pathway for sustainable power generation across various applications, including lighting and IoT sensor nodes.

Introduction

The growing demand for sustainable and autonomous power solutions, particularly in remote or off-grid environments, has driven significant interest in energy-harvesting technologies [1–5]. Energy harvesting techniques are generally categorized by their source: photovoltaic systems utilize sunlight [6], while electromagnetic generators (EMGs) [7], piezoelectric devices [8] and Triboelectric nanogenerators (TENGs) which convert mechanical motion into electricity. There are pros and cons for each energy harvesting method. For example, photovoltaics are limited in low-light environments, EMGs require bulky components and high wind speeds [9], while Piezoelectric and TENG harvesters typically produce low-power outputs and are sensitive to environmental conditions [10,11].

TENGs offer several advantages over traditional energy harvesting technologies. They can achieve high energy conversion efficiencies, with some designs demonstrating efficiencies between 50 % and 85 %. TENGs are effective at harvesting low-frequency mechanical energies, such as human motion and environmental vibrations, which are typically challenging for piezoelectric and EMG harvesters [12–15]. TENGs have gained prominence due to their ability to convert low-frequency and low-intensity mechanical stimuli into electrical energy without the need for external power sources [16].

TENGs' unique advantages—including low cost, simple structure, lightweight materials, and high compatibility with diverse substrates—make them highly suitable for powering wearable electronics, wireless sensor networks, and structural health monitoring systems in self-powered Internet of Things (IoT) applications [17,18]. TENGs operate based on triboelectrification and electrostatic induction and can be classified into four main working modes: contact-separation, sliding, freestanding triboelectric layer, and single-electrode mode [13]. This variety allows them to adapt to different mechanical excitation types [3,19]. Several works have achieved promising results with rotational TENGs, reaching power densities up to 8.55 mW/cm^2 [20] and 3.18 mW/cm^2 [21]. While these designs benefit from continuous contact forces, they often depend on sustained airflow and rotational motion, which may not be efficient in all environments [22–27].

Vibration-based sources—including building sway, ocean waves, and flow-induced vibrations—also present vast potential for mechanical energy harvesting [28]. Research into structures inspired by trees [29]

* Corresponding author.
E-mail address: a.ghaderiaram@tudelft.nl (A. Ghaderiaram).

https://doi.org/10.1016/j.ecmx.2025.101037
Received 14 February 2025; Received in revised form 29 March 2025; Accepted 22 April 2025
Available online 25 April 2025

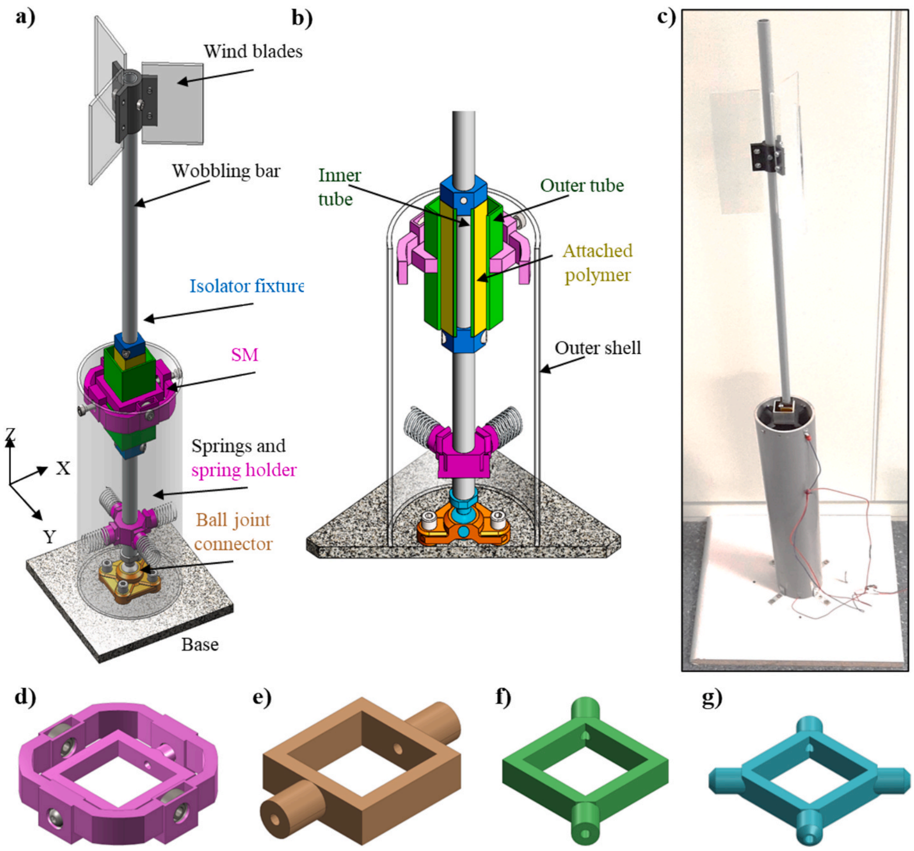

Fig. 1. Sketch of the WTENG **a)** Schematic of the entire structure, **b**) Cross-sectional view illustrating the contact-separation TENG details, **c**) Entire assembled structure. Schematic of SM **d**) gyroscope, **e**) normal hinge, **f**) rhombic hinge, and **g**) fixed.

or vortex-induced oscillations [30] shows that oscillating mechanisms can improve output performance. However, current works require a continuous flow of air or vibration. Integrating an unbalanced mass into vibration energy harvesting systems can significantly enhance energy conversion efficiency by amplifying small ambient vibrations. This approach utilizes rotational inertia to increase oscillatory motion, thereby improving the system's responsiveness to external excitations. For instance, a study demonstrated that a nonlinear double-mass pendulum energy harvester effectively captures low-frequency vibrations, showcasing the potential of unbalanced mass configurations in energy harvesting applications [31]. Additionally, research on the effects of proof mass geometry in vibration energy harvesters indicates that different geometrical dimension ratios significantly impact the resonance frequency and output performance, highlighting the importance of mass distribution in optimizing energy harvesting devices [32]. Unbalanced masses are utilized in TENGs to enhance energy harvesting efficiency, for example, a 3D chiral network of TENGs designed to effectively harvest water wave energy. This network employs chiral connections between unbalanced units, imparting flexibility and hyperelasticity in water, which enhances wave energy absorption and conversion [33]. An imbalance mass oscillation generator that converts kinetic energy from cardiac wall motion into electrical energy by oscillating in response to the heart's motion, generating power sufficient to operate medical implants like pacemakers [34]. However, there has been no research on using a wobbling mechanism that can be created by unbalanced beams (mass) and spring combinations for TENG energy harvesters. This can be very efficient in noncontinuous and small sources of wind and vibration applications.

To bridge this gap, this study introduces a Wobbling Triboelectric Nanogenerator (WTENG) that leverages a spring-supported, inverted pendulum mechanism to transition from a stable to an oscillatory state under minimal wind or vibration. This unbalanced configuration enables multi-directional motion and repeated contact separation, enhancing triboelectric performance without requiring continuous external force. The primary aim is to demonstrate the feasibility and key parameters (boundary conditions, electrode dimension, frequency of the input energy) affecting the performance of the proposed WTENG. This study further investigates impedance matching, rectification, and output optimization, demonstrating its potential as a practical energy harvesting solution for real-world application. A theoretical model was also developed for the wobbling-based mechanism to show the relationship between the leveraged contact force via inverted pendulum dynamics and evaluate impedance matching conditions for effective power transfer. These insights offer new design principles for low-frequency, multi-source energy harvesting systems.

Methods and materials

Working principle

Wobbling mechanism

In the depicted wobbling mechanism (see Fig. 1a), a bar is constrained by a ball joint connector to the base, allowing it to have half-spherical movement. Four springs are positioned to maintain the bar perpendicular to the base. At the top of this bar, three blades are mounted to capture the wind's mechanical energy from all directions and deflect the bar toward the direction of the wind. Consequently, the bar undergoes angular wobbling motion induced by the wind and the reaction of the springs.

Fig. 1b illustrates a contact-separation TENG that is positioned in the middle of the wobbling bar, consisting of two electrodes: an outer tube and an inner tube. A layer of Kapton is affixed to the outer surface of the

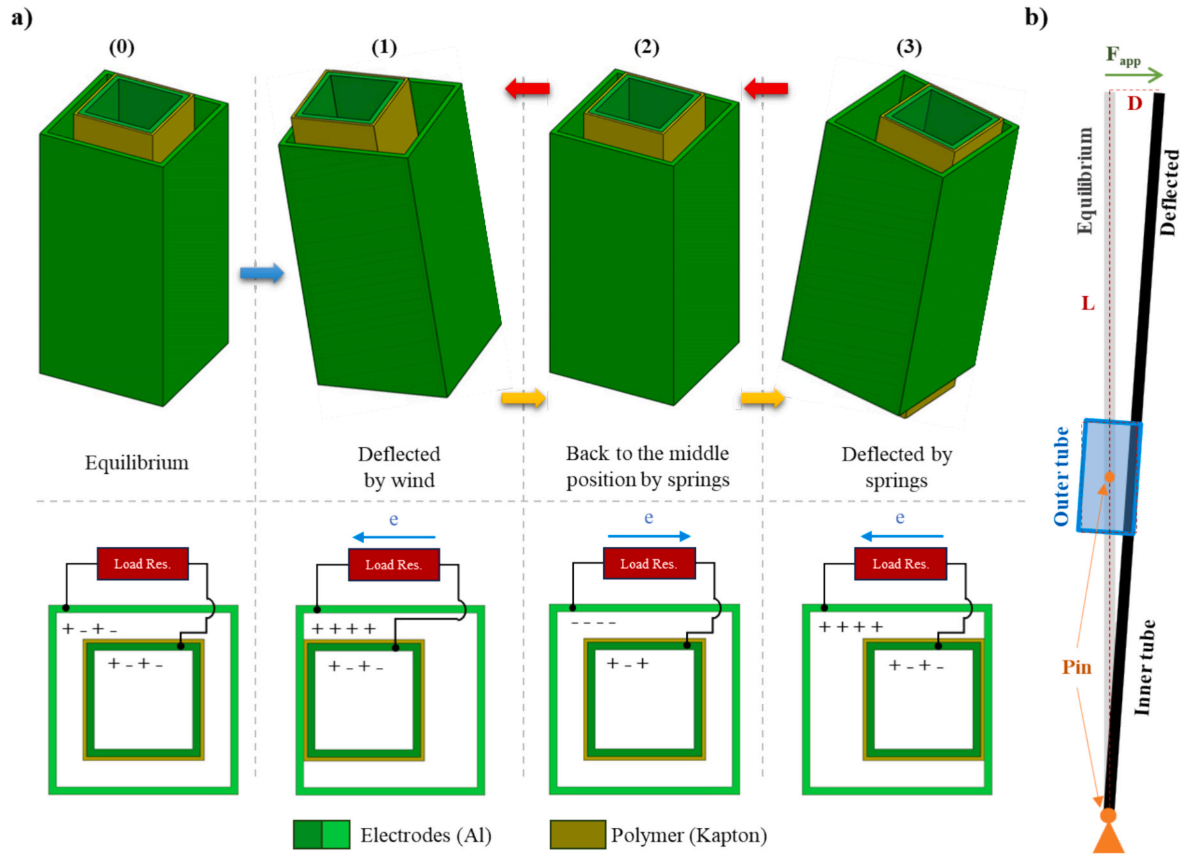

Fig. 2. **a)** Different states of WTENG and illustration of electric charge current. For each state, the top view of WTENG and its electrical condition is depicted at the bottom. **b)** Schematic of tube displacements in deflection mode.

Table 1
WTENG specifications, material configurations, and test parameters.

Test category	Material	variety	Note
Wobbling structure	3D-printed PLA SMs	Gyroscope Normal hinge Rhombic hinge Fixed	• Wobbling direction: 0, 90, 45 degrees. • Wobbling amplitude: 1–4 mm. • Wobbling frequency: 1–7 Hz.
TENG	Triboelectrification layers Outer electrode	Kapton Aluminum Aluminum tube	Thickness = 40 μm Thickness = 1.5 mm Cross section = square Width = 2.5 mm Length = 1.25 ~ 80 cm
	Inner electrode	Aluminum tube	Cross section = square Width = 1.5, 2 mm Length = 1.25–80 cm
Electrical performance		Open circuit voltage Power transmission Battery charging current	 R = 100 Ω–10 MΩ

inner tube, serving as the triboelectrification layer in contact with the inner surface of the outer tube. Two isolator fixtures position the inner tube at the bar's midpoint. Similarly, the outer tube is suspended in the same position but connected to the outer shell, utilizing a gyroscope structure to track the bar's movements when it comes into contact with the inner tube. The electrodes are connected to conductive wires for electrical connections, which are depicted in Fig. 1c.

Since the outer electrode encircles the inner electrode, the wobbling amplitude is restricted by the gap between the two electrodes. Describing the contact-separation process, when the wind pushes the blades, the bar deflects and the two electrodes come into contact. With a slight decrease in wind pressure, the tensioned and compressed springs push the bar back, separating the electrodes. Following this, the springs induce a wobbling movement, resulting in multiple reciprocating contact and separation events. The direction of the wind determines which surfaces of the electrodes come into contact. If the wind direction is parallel to the X or Y coordinates (Fig. 1a), only one surface of each electrode contacts. However, any combination of these two directions results in two surfaces of each electrode coming into contact. Additionally, the angle of the blowing wind affects the impact of contact on each paired surface. As a rough estimate, a larger contacting area would result if the wind pushes the blades at a 45-degree angle to the X and Y directions, assuming the same pressing force in both directions. It is important to note that the contacting force contributes to the effective contacting surface area at the nanoscale.

For suspending the outer electrode in position, various suspending mechanisms (SM) with different degrees of freedom are designed, as depicted in Fig. 1d-g, to study the impact of degrees of freedom on electrical performance.

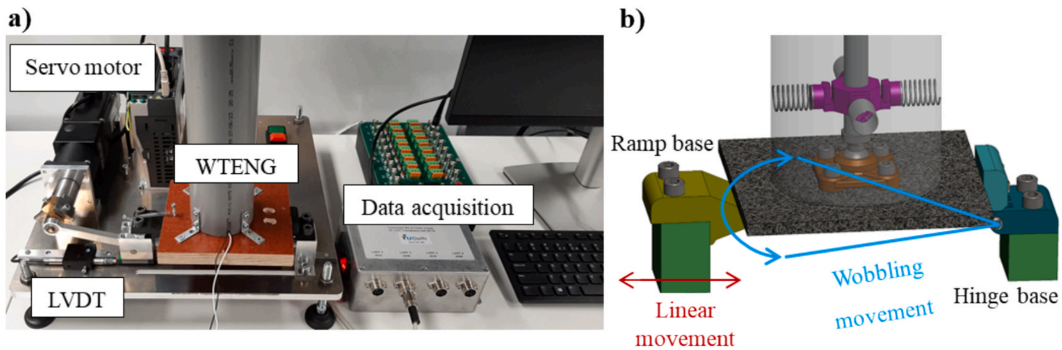

Fig. 3. **A)** Illustration of the entire test setup, and **b)** Schematic of converting horizontal movement to wobbling movements.

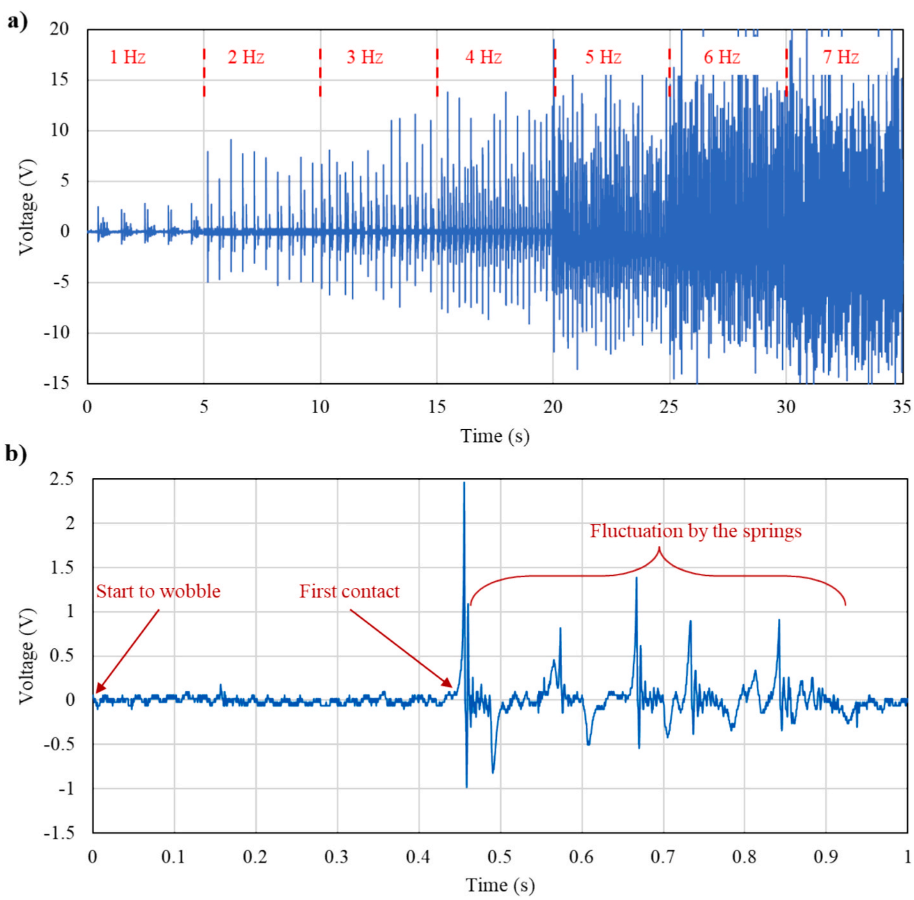

Fig. 4. Demonstration of experimental validation of the WTENG's working principle: **a)** Output voltage plotted against time for seven wobbling frequencies. **b)** Close-up of a single cycle of the 1 Hz wobbling.

Triboelectrification

Triboelectrification occurs when two heterogeneous materials come into contact, resulting in the transfer of electric charges between their surfaces. Upon separation, due to the characteristics of the materials and the speed of separation, some of the transferred charges remain on the respective surfaces, creating a localized static electric field [3,35]. Hence, both the contacting force and separation speed play crucial roles in determining the electrical performance.

To elucidate the electric charge generation process, a similar approach to references [36–38] is adopted. Fig. 2a illustrates the four mechanical and electrical states of WTENG. The four schematics at the bottom depict the top view of WTENG in different states with electric charge flow. State (0) represents equilibrium, wherein the wobbling bar is perpendicular to the base, and no contact occurs between the dynamic parts of WTENG, i.e. the inner electrode with attached polymer and outer electrode.

When the wobbling bar deflects (state 1), the outer electrode and polymer come into contact. Due to the higher negative triboelectric charge density of Kapton, electrons transfer from the aluminum electrode to Kapton to establish a balance between the occupied surface charge density in the outer electrode and Kapton [3,39]. Once these charge transfers occur, the outer electrode experiences a deficit of electrons, resulting in the movement of electrons through the load resistor (Fig. 2a) to maintain an equilibrium of charges.

Upon contact, the stored reaction force in the springs pushes the wobbling bar back, leading to separation in the WTENG (state 2). As separation commences, some transferred charges remain on Kapton's surface, generating a local electrostatic field[40]. This field attracts

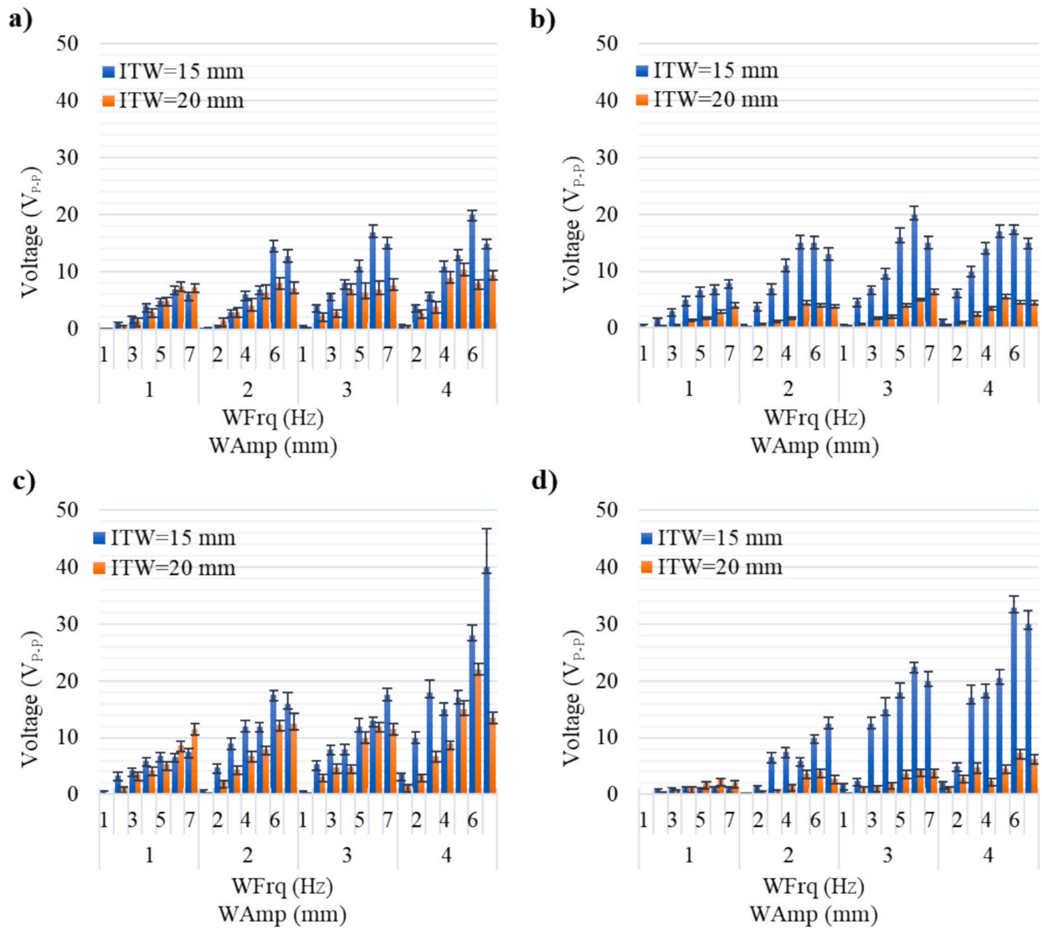

Fig. 5. Comparing the output voltage as a function of wobbling frequency and amplitude for ITW 15 and 20 mm, with **a)** TL of 800 mm using a normal hinge SM, **b)** TL of 800 mm using a gyroscope SM, **c)** TL of 200 mm using a normal SM, and **d)** TL of 200 mm using a gyroscope SM.

positive charges in the inner electrode toward Kapton, inducing a negative charge on the inner electrode. Consequently, charges tend to move toward the outer electrode through the load resistor to achieve a state of equilibrium. The magnitude of this current depends on the electrostatic field, which is determined by the amount of trapped charge on the Kapton surface, the dielectric coefficient and the thickness of Kapton, which has an inverse relationship with the thickness squared $\left(E = \frac{1}{4\pi\varepsilon_0}\frac{Q}{d^2}\right)$ where E is the electric field, Q is the electric charge in the distance d and ε_0 is the vacume permittivity (8.85×10^{-12} F·m^{-1}). Therefore, it is expected that the amplitude of the backward flow will be less than the contacting process.

Continuing from the reaction of the springs, the wobbling bar deflects in the opposite direction, resulting in contact in the WTENG, as depicted in Fig. 2a state (3). State (3) is similar to state (1) due to the square cross-section of the aluminum tubes and the uniform thickness of the attached polymer around the inner tube. The only difference lies in the force and speed of contact, which are expected to be lower than in state (1). The wobbling process will persist, oscillating between states (1-2-3-2-1) until it achieves an equilibrium state (0). This cyclical motion results in an alternating current in the load resistor. However, owing to damping in the wobbling, the generated current also exhibits a damping profile.

In addition to the contacting surface area, the contact force plays a crucial role in triboelectrification, as a higher impact force leads to more effective atomic-scale contact between surfaces [41]. The wobbling mechanism enhances this impact force by leveraging the inner bar's moment arm, as described by Equation (1):

$$M = F_{app}.L_i \qquad F_{PO} = F_{app}\frac{L_i}{L_{PO}} \tag{1}$$

where M is the moment at the bottom of the inner tube (near the ball joint) in Nm, F_{app} is the applied force (N), and L_i is the total length of the inner tube, as depicted in Fig. 2b. The force at the midpoint of the inner tube, F_{PO}, where the outer tube is positioned (L_{PO}), is twice as large because the moment arm is halved. This force amplification can be further increased by lowering the outer tube's position, but this also results in a larger maximum deflection (D, defined in Fig. 2b). The geometrical relationships governing this deflection are given in Equations 2–4:

$$\delta_{max} = \begin{cases} \dfrac{w_O - (2 \times t_O) - w_i}{2}, ifSM = fix \\ w_O - (2 \times t_O) - w_i, ifSM = pinned \end{cases} \tag{2}$$

$$\theta = \tan^{-1}\left(\frac{\delta_{max}}{\frac{L_i}{2} + \frac{L_O}{2}}\right) \tag{3}$$

$$D = L_i \times \tan(\theta) \tag{4}$$

where w_O, w_i and L_O represent the width and length of the outer and inner tubes, respectively, and δ_{max} is the maximum lateral displacement at the top of the outer tube. For a fixed SM, the lateral displacement is half that of a pinned SM, as rotation freedom affects the deflection

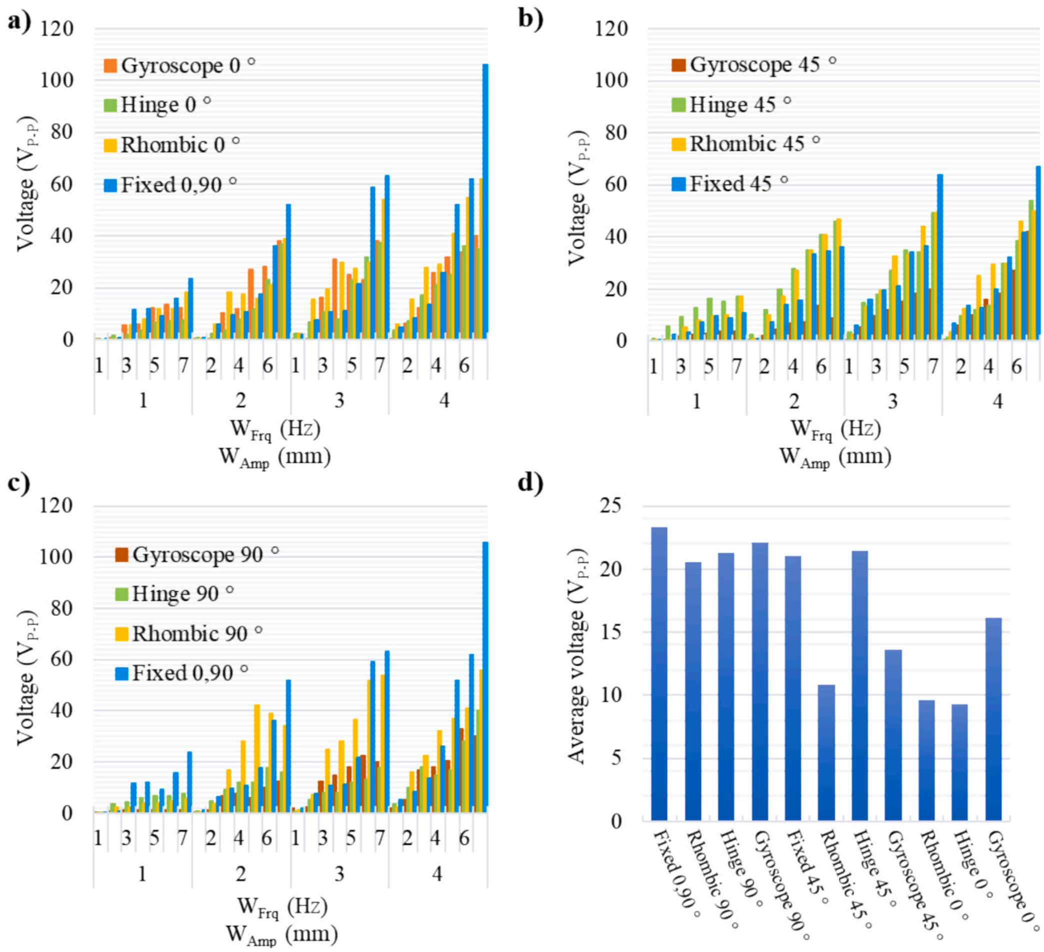

Fig. 6. Generated voltage of the WTENG using different SM and three wobbling directions **a)** parallel, **b)** diagonal and **c)** perpendicular to the rotating coordinate of the SM, plotted against variations in wobbling frequency and amplitude. **d)** presents a comparison of the average generated voltages across the three directions for each SM.

direction. Additionally, for diagonal movements, the lateral displacement is $\sqrt{2}$ times greater than for movements along the X or Y axis.

Since the full cycle of wobbling motion causes the top of the inner tube to travel a total distance of 2D, lowering the outer tube increases the wobbling cycle duration. This is because the inner tube requires more time to reach the outer tube, and stronger restoring springs are needed to return it to its equilibrium position.

Dynamic behavior of the wobbling system

The wobbling motion of the system can be modeled as a simple harmonic oscillator, governed by Newton's Second Law. Since the force acting on the system is cyclic, the acceleration follows $F = ma$ where m is the effective mass of the wobbling object and $a = \frac{d^2x}{dt^2}$ is the acceleration of the object in x displacement in time t. The system's restoring force is characterized by an effective stiffness k, leading to the equation of motion (Equation (5):

$$m\frac{d^2x}{dt^2} + kx = 0 \tag{5}$$

which is a second-order homogeneous differential equation describing simple harmonic motion. The natural angular frequency of the system ω_n is given by Equation (6):

$$\omega_n = \sqrt{\frac{k}{m}} \tag{6}$$

which defines the fundamental oscillation frequency of the system when displaced from equilibrium. Solving the differential equation and assuming an initial displacement x_0 and initial velocity υ_0, the system's motion follows Equation (7):

$$x(t) = x_0\cos(\omega_n t) + \frac{\vartheta_0}{\omega_n}\sin(\omega_n t) \tag{7}$$

where x(t) describes the displacement of the inner tube over time. Since the full-cycle wobbling movement is defined as 2D and is time-dependent, the optimal energy transfer occurs when the excitation frequency matches the natural frequency.

Since the effective stiffness k can be expressed in terms of force and displacement as $k = \frac{F}{D}$, the natural frequency, expressed in Hertz, is given by Equation (8):

$$f_n = \frac{\omega_n}{2\pi} = \frac{1}{2\pi}\sqrt{\frac{F}{mD}} \tag{8}$$

This equation demonstrates that the optimal wobbling frequency is determined by the applied cyclic force, the effective mass of the system, and the displacement range, which is influenced by the tube dimensions. If the system is driven at its natural frequency by an external force, resonance occurs, leading to maximum oscillation amplitude and high-efficiency cyclic contact-separation events. Therefore, accurately understanding the system's natural frequency is essential for optimizing the wobbling triboelectric nanogenerator's energy-harvesting performance.

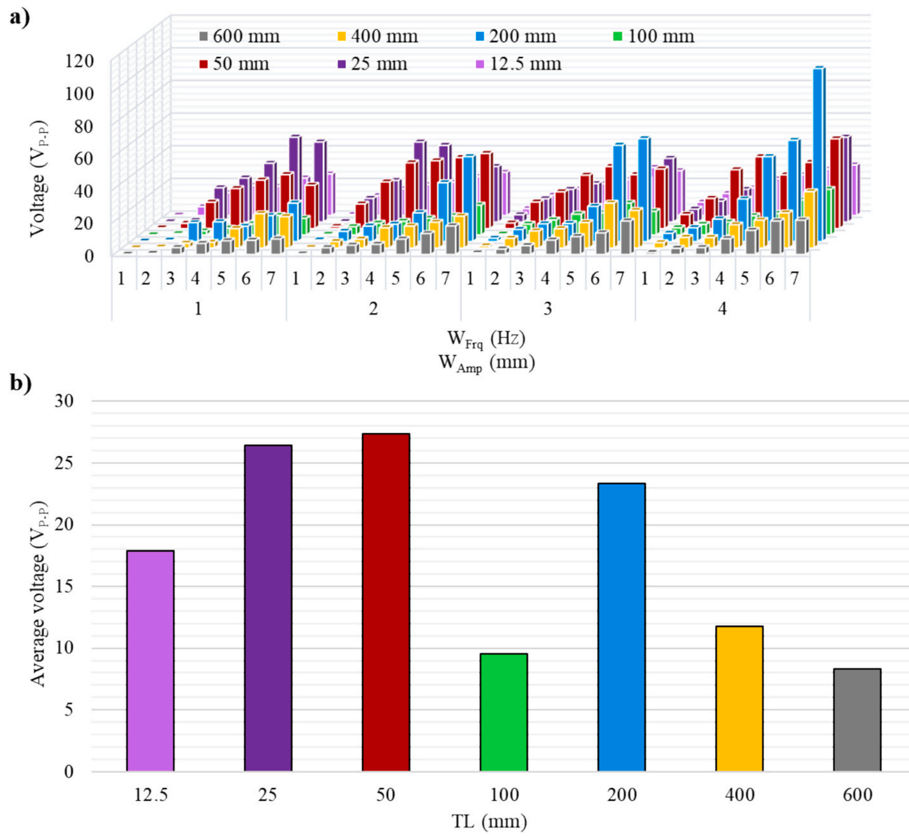

Fig. 7. **a**) Comparison of the generated voltage as a function of wobbling amplitude and frequency using fixed SM and different TLs, **b**) Comparison of the average generated voltage for the fixed SM across various TLs.

Dynamic behavior of WTENG's impedance

The electrical characteristics of the WTENG are influenced by the contact mechanics of its wobbling motion. As established in the previous section, increased excitation—especially near the natural frequency of the system—results in greater acceleration, which in turn enhances the contact force between the electrodes. This increase in contact force plays a critical role in shaping the WTENG's intrinsic impedance.

A higher contact force leads to more intimate contact and a smaller electrode gap. Since the capacitance in a parallel-plate model is inversely proportional to the distance between them $\left(C \propto \frac{1}{distance}\right)$, where C is the capacitance, a reduced gap results in higher effective capacitance [42]. Additionally, during rapid separation, the rate of electrode disengagement increases, which limits the time window for charge dissipation through tunneling or air breakdown when the gap is minimal. This dynamic behavior helps preserve the generated charges and contributes to efficient energy transfer [43].

From an electrical standpoint, the capacitive impedance (Z_C) of the WTENG, given by $\left(Z_C = -j\frac{1}{2\pi fC}\right)$, where f and C are signal frequency and capacitance, decreases as capacitance increases. This means that under stronger contact force conditions, the WTENG exhibits lower internal impedance, allowing more efficient power delivery to the external circuit. When the load resistance is properly matched to this internal impedance, conjugate impedance matching is achieved, resulting in maximal power transfer [44]. Understanding the dynamic relationship between mechanical contact force and electrical impedance is therefore essential for optimizing load conditions, especially when the WTENG operates under variable mechanical excitation.

Rectifier impedance and power transfer efficiency

To enable energy storage, the WTENG is connected to a rectification circuit consisting of a diode bridge and a 3.7 V lithium-ion battery. The rectifier's dynamic impedance plays a critical role in determining the power transfer efficiency from the WTENG to the storage element. It can be approximated by Ohm's law as Equation (9).

$$R_{DB} = \frac{V_f}{I_f} \tag{9}$$

where V_f is the total forward voltage drop of the conducting diodes and I_f is the average charging current. In a typical silicon diode bridge, each diode introduces a forward voltage drop of approximately 0.7 V, leading to a combined drop of 1.4 V during conduction.

To ensure efficient energy transfer to the storage unit, the rectification circuit should present an input impedance that aligns with the WTENG's dynamic output impedance. This impedance compatibility facilitates conjugate matching, minimizing power loss and enabling effective battery charging. Therefore, impedance considerations in the rectifier design are essential for maintaining overall system efficiency.

Material

The electrodes of the WTENG are made from industrial-grade aluminum tubes with detailed information regarding their dimensions provided in Table 1. The polymer used is a polyamide (Kapton) film with one-side adhesion and a thickness of 40 µm, possessing a triboelectric charge density of -92.88 µcm^{-2} [39]. The triboelectric charge density for Al_2O_3 is -1.5 µcm^{-2} [45] which makes a significant contrast for a higher triboelectrification in the contact-separation process. Furthermore, both materials are commercially available, require no additional surface treatment, and eliminate the need for complex fabrication processes, making them highly scalable for energy-harvesting applications. For the wobbling structure, an aluminum bar with a diameter of 10 mm was selected due to its lightweight properties. The ball joint used is a

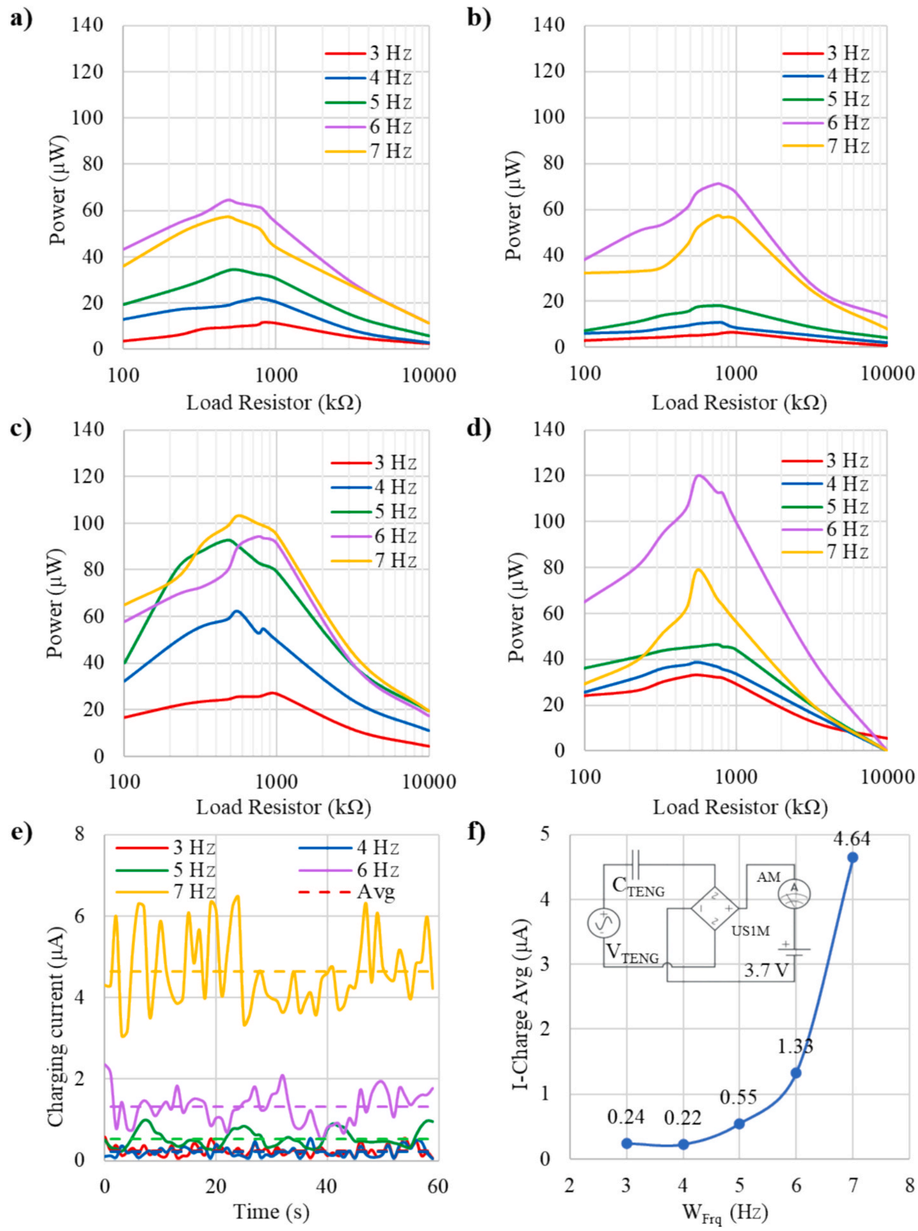

Fig. 8. *Electric power generation at wobbling frequencies and amplitudes of 1–4 mm (**a** − **d**). **e)** Battery charge current profile with varying frequency and 3 mm amplitude over time. **f)** Average charge current at 3 mm amplitude vs. frequency, with battery charging circuit diagram inset.*

cost-effective variant commonly found in chair bases. A Polyvinylchloride (PVC) drain pipe with a diameter of 75 mm serves as the outer shell. All mechanical connectors, such as the gyroscope, wind blade holder, springs holder, and isolator fixture, are 3D printed from a tough Polylactic acid (PLA) material. Additionally, to ensure smooth and low-resistance operation of the gyroscope, four small ball bearings are incorporated into the joints. In material selection, prioritizing cost-effectiveness and ease of availability and use was paramount to align with the core principles of triboelectric energy harvesting.

Test method and effective parameters investigated

The test method involves inducing wobbling through wind force. However, controlling wind in a laboratory setting requires expensive equipment and facilities. Given that WTENG can harvest any type of wobbling movement, it is decided to induce wobbling by moving the base rather than the wobbling bar. Comparing the movements in these two conditions (wobbling the bar or the base) yields the same results, as ultimately, the wobbling bar with all its installed parts moves against the fixed components installed on the outer shell and base. Therefore, wobbling the base can be achieved under controlled conditions using the designed setup shown in Fig. 3a.

The operating principle of the setup is that a servo motor provides precise and controlled rotation, while a reciprocating mechanism converts these rotational movements into linear movements. Additionally, a linear guide ensures perfect one-dimensional linearity. As depicted in Fig. 3b, the wobbling structure is installed on two bases: the hinge base, which is fixed and allows for angular movements, and the ramp base, which is connected to the reciprocating part and converts horizontal movement into vertical displacements. Consequently, the back-and-forth movements of the ramp base result in the wobbling of the WTENG.

Using this setup enables the control and testing of all parameters represented in Table 1, which contribute to electrical output performance. A Linear Variable Differential Transformer (LVDT) is incorporated to measure linear movements, which correlate linearly with the wobbling angle according to the Pythagorean principle. Additionally, to capture electrical parameters, a digital oscilloscope and an ammeter are utilized.

Results and discussions

Fig. 4a plots the output voltage over time for seven different wobbling frequencies, all with a wobbling amplitude of 3 $mm_{p\text{-}p}$, an outer tube width (OTW) of 25 mm, an inner tube width (ITW) of 15 mm and a tube length (TL) of 25 mm. The graph demonstrates an increase in output voltage with increasing the wobbling frequency. This phenomenon can be attributed to the rise in contact force, as it is described in the dynamic behaviour of the wobbling system. Since the mass of the wobbling bar remains constant, an increase in acceleration results in a higher force.

To look deeper into the working principle, Fig. 4b provides a zoomed-in view of a single cycle of 1 Hz wobbling. This figure highlights the fluctuation process occurring due to the spring's reaction force. However, owing to the low speed of the external wobbling, these fluctuations become damped over time through several contact and separation events.

As per the TENG's principle, greater contact area results in increased triboelectrification and higher electricity generation[46]. To assess this and determine the optimal TL and difference in tube widths, a series of tests with various dimensions are conducted. Another important factor that is evaluated is the SM (Fig. 1d-g), as the degree of freedom impacts the spring-based fluctuations, where a more rigid mechanism provides a greater impact energy during the time of contact. In order to evaluate the optimal WTENG size, experiments are conducted with different SMs. Additionally, to account for the influence of TL and difference in tube widths on electrical performance, experiments are carried out with two ITWs (15 and 20 mm) and two TLs (200 and 800 mm) for each SM.

Comparing the two different ITWs in Fig. 5 reveals that ITW = 15 mm exhibits a better performance in both normal hinge and gyroscope SMs, across the long and short TLs. Surprisingly, Fig. 5c and 5d demonstrate that a shorter TL leads to a higher output voltage, contrary to the expectation of "higher contacting area, higher performance". The error bars in Fig. 5 show the variation in the amplitude of output voltage in repetitive wobbling motion. Based on these findings, additional tests are done with ITW = 15 mm and TL = 200 mm to determine the optimal SM.

Given that the test setup only wobbles the WTENG in one direction (let's refer to it as direction X), it is important to acknowledge that real-world scenarios involve two-directional wobbling (directions X and Y). Moreover, the effect of wobbling direction influence on the WTENG's performance is investigated, including directions parallel, perpendicular, and diagonal to the rotating coordinate of the SM.

Fig. 6a-c illustrates the generated voltage of the WTENG using different SMs and three different wobbling directions, for the fixed SM, wobbling directions of 0 and 90 degrees are considered the same, across variations in wobbling frequency and amplitude. The variation in output voltage peaks in each test is in the range of 5 % to 17 % and the error bars are removed to avoid messi figure.

The results from different SMs are compared with the average generated voltages in all wobbling directions. As shown in Fig. 6d, the fixed SM provides the best performance. Despite the lack of degree of freedom in the fixed SM, the solid contact between dynamic parts of the WTENG contributes to a higher voltage output.

To determine the optimal TL, sets of experiments are conducted using a fixed SM and a wobbling direction perpendicular to SM's rotation coordinate and ITW = 15 mm. Fig. 7a illustrates the generated voltage as a function of wobbling amplitude and frequency utilizing different TLs. While increasing TL generally leads to a higher output voltage, it is noteworthy that the decrease in the surface flatness associated with longer TLs contributes to a reduction in the effective contact area.

Additionally, according to Equation (8), the natural frequency of the entire structure, which depends on the dimensions and weight of the wobbling structure, plays a role in generating the output voltage[47]. Consequently, at certain wobbling frequencies and amplitudes, the generated voltage can be significantly higher than the other TLs, irrespective of the speed-dependent contacting force. This factor adds another dimension of consideration alongside the contact area and needs further modeling and evaluation.

So far, optimization has been based on comparing the generated output, representing the harvested electric charges. However, since energy harvesting is the primary objective of designing the WTENG, the transmission and storage of electric power become important considerations in energy harvesters. To examine the electrical characteristics of the WTENG, a variety of resistors (0.1 to 10 MΩ) are applied as electrical loads, and the power consumption of the resistors is recorded at different wobbling frequencies and amplitudes (Fig. 8a-d) to find the maximum power transmission based on the explanation in the section of Dynamic behavior of WTENG's impedance.

Fig. 8a-d illustrates how the wobbling amplitude and frequency directly affect the WTENG's output performance. Considering the parameters TL = 50 mm and ITW = 15 mm, the generated power density at a wobbling amplitude of 4 mm and frequency of 6 Hz is 1.6 W/m^2. However, it is noticeable that in certain cases, such as Fig. 8a, and b, increasing the frequency from 6 to 7 Hz does not lead to a higher output. This phenomenon is attributed to the natural frequency of the wobbling mechanism.

To store the generated electric charges in a 3.7 V lithium-ion battery, a bridge diode made of ultra-fast recovery rectifier diodes (shown as an inset in Fig. 8f) was used to minimize voltage loss across components. Fig. 8e shows the time-dependent charging current measured during WTENG operation at different wobbling amplitudes. Due to the low sampling rate of the ammeter, the current profile appears non-repetitive. Nevertheless, based on the average measured current, Fig. 8f reveals an exponential-like increase in charging current with wobbling frequency. Based on Equation (9), at an average charging current of approximately 4.6 μA, the estimated rectifier impedance is about 300 kΩ, which closely aligns with the optimal load resistance obtained from power transmission tests (Fig. 8a–d). This match confirms that the diode bridge does not cause a significant impedance mismatch, supporting effective energy transfer to the battery and validating the rectification and storage strategy. In order to evaluate the functionality of the WTENG as an energy harvester, it is installed inside a light mast to charge the battery. The stored energy supplied a 0.1 W LED for a few seconds and only when the employed passive infrared (PIR) sensor detects human motion.

Conclusions

This research presents a new approach to harnessing wind energy by combining mechanical wobbling and TENG in order to provide a sustainable and cost-effective energy harvesting system to be used across different applications. Efficient energy harvesting capabilities have been demonstrated through the leveraging of wobbling motion and the utilization of a contact-separation mode TENG. The optimization of key parameters such as electrode dimensions, and wobbling mechanisms has led to significant improvements in power generation efficiency, about 1.6 W/m^2 for TL = 50 mm, ITW = 15 mm in wobbling frequency and amplitude of 6 Hz and 2 mm respectively. Experimental results have shown the effect of wobbling frequency, amplitude, and SM on output efficiency, building the ground for future research and development. The successful integration of the WTENG into a real-world application, e.g. charging a Li-ion battery with a charging current of 4.6 μA and supplying power to a light mast, demonstrated its practical viability. This study highlights the potential of WTENGs as sustainable and efficient solutions for diverse energy harvesting needs, particularly in IoT sensor nodes and other remote applications. Future research directions may include further optimization of WTENG design, scalability for large-scale deployment, and exploring additional practical applications across various industries. Another aspect that needs more investigation for optimum performance is engineering the entire system's natural frequency.

Limitations and future work

While the WTENG demonstrates promising energy-harvesting capabilities, several aspects require further investigation to ensure its practical deployment in real-world environments. One key limitation of this study is the lack of experimental evaluation under varying environmental conditions, such as humidity, temperature fluctuations, and long-term mechanical fatigue. Since triboelectric charge transfer can be influenced by surface contamination, moisture absorption, and material wear, future work should include controlled environmental testing to assess the WTENG's stability and efficiency over extended operation periods.

Additionally, material degradation over time remains an open question. Although Kapton and aluminum are widely used for their durability and resistance to chemical degradation, repeated contact-separation cycles may lead to surface wear, which could affect charge transfer efficiency. Investigating surface modifications or protective coatings could enhance the WTENG's lifespan while maintaining triboelectric performance.

Another limitation lies in structural optimization for different wind and vibration conditions. The wobbling mechanism in this study was designed to function under controlled laboratory settings, but in outdoor environments, wind turbulence, irregular vibrations, and external mechanical forces may introduce unpredictable variations in performance. Future studies should include wind tunnel experiments to validate the WTENG's response to real-world wind profiles, as well as improvements in blade design to enhance energy capture efficiency.

To achieve a more optimized WTENG design, future work should also include simulation-based and analytical investigations. Finite element modeling and computational fluid dynamics could provide deeper insights into the structural behavior, airflow interaction, and mechanical response of the system, helping to refine key parameters such as wobbling frequency, blade dimensions, and aerodynamic efficiency. Analytical modeling can further aid in establishing performance prediction frameworks and design guidelines to improve overall energy conversion efficiency.

Moreover, energy storage and power management are critical aspects that were not fully explored in this study. Although the WTENG was demonstrated to charge a Li-ion battery, an in-depth analysis of energy conversion efficiency, rectification losses, and storage system integration is necessary for developing fully autonomous self-powered systems.

Despite these limitations, this study provides a feasibility study for wobbling-based energy harvesting, offering a scalable and low-cost solution. Addressing these challenges through material enhancements, environmental testing, advanced simulations, blade design optimization, and real-world wind testing will be essential for deploying WTENG in practical applications such as structural health monitoring, wireless sensor networks, and off-grid energy solutions.

CRediT authorship contribution statement

Aliakbar Ghaderiaram: Writing – original draft, Methodology, Investigation, Conceptualization. **Erik Schlangen:** Supervision, Resources, Funding acquisition. **Mohammad Fotouhi:** Writing – review & editing, Supervision, Resources, Project administration, Funding acquisition.

Declaration of competing interest

The authors declare that they have no known competing financial interests or personal relationships that could have appeared to influence the work reported in this paper.

Acknowledgements

This research was supported by Janjaap Ruijssenaars from Gravity Energy Company, who provided the inverted pendulum–TENG combination and Timberlab Company, who provided both materials and technical advice for outdoor lighting.

Data availability

Data will be made available on request.

References

[1] Zhang M, et al. Mechanical energy harvesters with tensile efficiency of 17.4% and torsional efficiency of 22.4% based on homochirally plied carbon nanotube yarns. *Nat Energy* 2023;8(2):203–13. https://doi.org/10.1038/s41560-022-01191-7.

[2] Chen J, et al. Micro-cable structured textile for simultaneously harvesting solar and mechanical energy. Nat. Energy 2016;1(10):1–8. https://doi.org/10.1038/nenergy.2016.138.

[3] Zhang C, Wang ZL, Triboelectric Nanogenerators, pp. 1335–1376, 2018, doi: 10.1007/978-981-10-5945-2_38.

[4] Bănică MA. Energy harvesting from renewable energy sources. *Lect Notes Networks Syst*, 2020;85:247–54. https://doi.org/10.1007/978-3-030-26991-3_23.

[5] Nt Nb. Fk. E B. *Energy Harvesting and Energy Efficiency* 2017;vol. 37. https://doi.org/10.1007/978-3-319-49875-1.

[6] Ren J, et al. Light power resource availability for energy harvesting photovoltaics for self-powered IoT. *J Phys Energy* 2024;6:15018. https://doi.org/10.1088/2515-7655/ad1764.

[7] Beeby SP, O'Donnell T. Electromagnetic energy harvesting. Energy Harvest Technol 2009:129–61. 10.1007/978-0-387-76464-1_5.

[8] Toprak A, Tigli O. Piezoelectric energy harvesting: State-of-the-art and challenges Piezoelectric energy harvesting: state-of-the-art and challenges. *Appl. Phys. Rev.* 2014;1:31104. https://doi.org/10.1063/1.4896166.

[9] Tian J, Chen X, Wang ZL. Environmental energy harvesting based on triboelectric nanogenerators. *Nanotechnology* 2020;31(24):242001. https://doi.org/10.1088/1361-6528/AB793E.

[10] Ahmed A *et al.*, Triboelectric nanogenerator versus piezoelectric generator at low frequency (<4 Hz): a quantitative comparison, 2020, doi: 10.1016/j.isci.2020.101286.

[11] Callaty C, Rodrigues C, Ventura J. Triboelectric nanogenerators in harsh conditions: a critical review. *Nano Energy* 2025;135:110661. https://doi.org/10.1016/J.NANOEN.2025.110661.

[12] Wang ZL. Triboelectric nanogenerators as new energy technology and self-powered sensors - principles, problems and perspectives. *Faraday Discuss*, 2014;176:447–58. https://doi.org/10.1039/C4FD00159A.

[13] Xie Y, et al. Grating-structured freestanding triboelectric-layer nanogenerator for harvesting mechanical energy at 85% total conversion efficiency. *Adv Mater*, Oct. 2014;26(38):6599–607. https://doi.org/10.1002/ADMA.201402428.

[14] Cheng T, Gao Q, ZL Wang, The current development and future outlook of triboelectric nanogenerators: a survey of literature, *Adv Mater Technol*, 4 (3), 2019, 10.1002/ADMT.201800588.

[15] Wang X, et al. A double-float structured triboelectric nanogenerator for wave hydrological monitoring. *Sustain Energy Technol Assessm.* 2022;54:102824. https://doi.org/10.1016/J.SETA.2022.102824.

[16] Wang ZL. Triboelectric nanogenerators as new energy technology for self-powered systems and as active mechanical and chemical sensors. *ACS Nano* 2013;7(11):9533–57. https://doi.org/10.1021/NN404614Z/ASSET/IMAGES/LARGE/NN-2013-04614Z_0018.JPEG.

[17] Qin Y, Fu X, Lin Y, Wang Z, Cao J, Zhang C. Self-powered Internet of Things sensing node based on triboelectric nanogenerator for sustainable environmental monitoring. *Nano Res*, 2023;16(9):11878–84. https://doi.org/10.1007/S12274-023-5689-8/METRICS.

[18] Zhu M, Yi Z, Yang B, Lee C. Making use of nanoenergy from human – Nanogenerator and self-powered sensor enabled sustainable wireless IoT sensory systems. *Nano Today* 2021;36:101016. https://doi.org/10.1016/J.NANTOD.2020.101016.

[19] Wardhana EM, et al. Harvesting contact-separation-compression vibrations using a flexible and compressible triboelectric generator. *Sustain Energy Technol Assessm* Dec. 2020;42:100869. https://doi.org/10.1016/J.SETA.2020.100869.

[20] Ghaderiaram A, Bazrafshan A, Firouzi K, Kolahdouz M. A multi-mode R-TENG for self-powered anemometer under IoT network. *Nano Energy* 2021;87:106170. https://doi.org/10.1016/J.NANOEN.2021.106170.

[21] Zhu G, Chen J, Zhang T, Jing Q, Wang ZL. Radial-arrayed rotary electrification for high performance triboelectric generator. Nat Commun 2014;5(1):1–9. https://doi.org/10.1038/ncomms4426.

[22] Long L, et al. High performance floating self-excited sliding triboelectric nanogenerator for micro mechanical energy harvesting. *Nat Commun* 2021;12(1):1–10. https://doi.org/10.1038/s41467-021-25047-y.

[23] Li J, Cheng L, Wan N, Ma J, Hu Y, Wen J. Hybrid harvesting of wind and wave energy based on triboelectric-piezoelectric nanogenerators. *Sustain Energy Technol Assessments* 2023;60:103466. https://doi.org/10.1016/J.SETA.2023.103466.

[24] Deng W, et al. Ternary electrification layered architecture for high-performance triboelectric nanogenerators. *ACS Nano* 2020;14(7):9050–8. https://doi.org/10.1021/ACSNANO.0C04113/ASSET/IMAGES/LARGE/NN0C04113_0006.JPEG.

[25] Feng Y, Zhang L, Zheng Y, Wang D, Zhou F, Liu W. Leaves based triboelectric nanogenerator (TENG) and TENG tree for wind energy harvesting, 2018, doi: 10.1016/j.nanoen.2018.10.075.

[26] Huang L-B, Xu W, Bai G, Wong M-C, Z. Yang, J. Hao, Wind energy and blue energy harvesting based on magnetic-assisted noncontact triboelectric nanogenerator, 2016, 10.1016/j.nanoen.2016.09.032.

[27] Ahmed A, Hassan I, Hedaya M, El-Yazid A, J. Zu, Z. L. Wang, Farms of triboelectric nanogenerators for harvesting wind energy: a potential approach towards green energy, 2017, doi: 10.1016/j.nanoen.2017.03.046.

[28] Sun R, Zhou S, Cheng L. Ultra-low frequency vibration energy harvesting: Mechanisms, enhancement techniques, and scaling laws. *Energy Convers Manag*, 2023;276:116585. https://doi.org/10.1016/J.ENCONMAN.2022.116585.

[29] Zeng Q, et al. A high-efficient breeze energy harvester utilizing a full-packaged triboelectric nanogenerator based on flow-induced vibration. *Nano Energy* 2020;70: 104524. https://doi.org/10.1016/J.NANOEN.2020.104524.

[30] Zhang L, et al. Vortex-induced vibration triboelectric nanogenerator for low speed wind energy harvesting. *Nano Energy* 2022;95:107029. https://doi.org/10.1016/J.NANOEN.2022.107029.

[31] Cai Q, Zhu S. Nonlinear double-mass pendulum for vibration-based energy harvesting. *Nonlinear Dyn* 2024;112(7):5109–28. https://doi.org/10.1007/S11071-023-09236-6/FIGURES/20.

[32] Alameh AH, Gratuze M, Elsayed MY, Nabki F. Effects of proof mass geometry on piezoelectric vibration energy harvesters. Sensors 2018;18(5):1584. https://doi.org/10.3390/S18051584.

[33] Li X, et al. Three-dimensional chiral networks of triboelectric nanogenerators inspired by metamaterial's structure. *Energy Environ Sci* 2023;16(7):3040–52. https://doi.org/10.1039/D3EE01035J.

[34] Zurbuchen A, et al. Energy harvesting from the beating heart by a mass imbalance oscillation generator. *Ann Biomed Eng* 2013;41(1):131–41. https://doi.org/10.1007/S10439-012-0623-3.

[35] Gao Y, He L, Liu D, Zhang J, Wang ZL, Wang J. Spontaneously established reverse electric fi eld to enhance the performance of triboelectric nanogenerators via improving Coulombic ef fi ciency, pp. 1–11, 2024, 10.1038/s41467-024-48456-1.

[36] Zhao H, et al. Theoretical modeling of contact-separation mode triboelectric nanogenerators from initial charge distribution. *Energy Environ Sci* 2024;17:2228. https://doi.org/10.1039/d3ee04143c.

[37] Zhang H, et al. A general optimization approach for contact-separation triboelectric nanogenerator. *Nano Energy* 2019;56:700–7. https://doi.org/10.1016/J.NANOEN.2018.11.062.

[38] Niu S *et al.*, Theoretical study of contact-mode triboelectric nanogenerators as an effective power source, 10.1039/c3ee42571a.

[39] Zou H, et al. Quantifying the triboelectric series. Nat Commun 2019;10(1):1–9. https://doi.org/10.1038/s41467-019-09461-x.

[40] Kwak SS, et al. Triboelectrification-induced large electric power generation from a single moving droplet on graphene/polytetrafluoroethylene. *ACS Nano* 2016;10 (8):7297–302. https://doi.org/10.1021/ACSNANO.6B03032/ASSET/IMAGES/LARGE/NN-2016-03032A_0005.JPEG.

[41] Inoue K, Suzuki A, Mitsui T. From contact electrification to triboelectric nanogenerators, 2007, 10.1088/1361-6633/ac0a50.

[42] Dharmasena RDIG, Deane JHB, Silva SRP. Nature of power generation and output optimization criteria for triboelectric nanogenerators. *Adv Energy Mater*, 2018;8 (31):1802190. https://doi.org/10.1002/AENM.201802190.

[43] Wang J *et al.*, Achieving ultrahigh triboelectric charge density for efficient energy harvesting, *Nat Commun 8(1)*, 1–8, 2017, 10.1038/s41467-017-00131-4.

[44] Liu S, et al. A self-powered gas sensor based on coupling triboelectric screening and impedance matching effects. *Adv Mater Technol*, 2021;6(12):Dec. https://doi.org/10.1002/ADMT.202100310.

[45] Zou H, et al. Quantifying and understanding the triboelectric series of inorganic non-metallic materials. *Nat Commun*, 2020;11(1):1–7. https://doi.org/10.1038/s41467-020-15926-1.

[46] Cheng T, Shao J, Wang ZL. Triboelectric nanogenerators. Nat Rev Methods Prim 2023;3(1):1–13. https://doi.org/10.1038/s43586-023-00220-3.

[47] Ganapathy SR, Salleh H, Azhar MKA. Design and optimisation of magnetically-tunable hybrid piezoelectric-triboelectric energy harvester. Sci Rep 2021;11(1): 1–13. https://doi.org/10.1038/s41598-021-83776-y.